THE JOURNAL OF BIOLOGICAL CHEMISTRY VOL. 288, NO. 14, pp. 9755–9766, April 5, 2013


# Three-dimensional Structure of *Saccharomyces* Invertase

## *ROLE OF A NON-CATALYTIC DOMAIN IN OLIGOMERIZATION AND SUBSTRATE SPECIFICITY**

Received for publication, December 20, 2012, and in revised form, February 20, 2013 Published, JBC Papers in Press, February 21, 2013, DOI 10.1074/jbc.M112.446435

**M. Angela Sainz-Polo[‡1,2], Mercedes Ramírez-Escudero[‡1], Alvaro Lafraya[§3], Beatriz González[‡], Julia Marín-Navarro[§], Julio Polaina[§], and Julia Sanz-Aparicio[‡4]**

*From the [‡]Departamento de Cristalografía y Biología Estructural, Instituto de Química-Física "Rocasolano," Consejo Superior de Investigaciones Científicas (CSIC), Serrano 119, 28006 Madrid and the [§]Instituto de Agroquímica y Tecnología de Alimentos, CSIC, 46980 Paterna, Valencia, Spain*

**Background:** Invertase is a fundamental enzyme for sugar metabolism in yeast and a classical model in early biochemical studies.
**Results:** Invertase shows an unusual octameric quaternary structure composed of two types of dimers.
**Conclusion:** A peculiar pattern of monomer assembly through non-catalytic domain interactions determines invertase specificity.
**Significance:** Unraveling the structural features that rule enzyme modularity casts new light on protein-carbohydrate recognition.

**Invertase is an enzyme that is widely distributed among plants and microorganisms and that catalyzes the hydrolysis of the disaccharide sucrose into glucose and fructose. Despite the important physiological role of *Saccharomyces* invertase (SInv) and the historical relevance of this enzyme as a model in early biochemical studies, its structure had not yet been solved. We report here the crystal structure of recombinant SInv at 3.3 Å resolution showing that the enzyme folds into the catalytic β-propeller and β-sandwich domains characteristic of GH32 enzymes. However, SInv displays an unusual quaternary structure. Monomers associate in two different kinds of dimers, which are in turn assembled into an octamer, best described as a tetramer of dimers. Dimerization plays a determinant role in substrate specificity because this assembly sets steric constraints that limit the access to the active site of oligosaccharides of more than four units. Comparative analysis of GH32 enzymes showed that formation of the SInv octamer occurs through a β-sheet extension that seems unique to this enzyme. Interaction between dimers is determined by a short amino acid sequence at the beginning of the β-sandwich domain. Our results highlight the role of the non-catalytic domain in fine-tuning substrate specificity and thus supplement our knowledge of the activity of this important family of enzymes. In turn, this gives a deeper insight into the structural features that rule modularity and protein-carbohydrate recognition.**

Invertase (EC 3.2.1.26; β-fructofuranosidase) catalyzes the hydrolysis of the disaccharide sucrose (table sugar) into glucose and fructose and is a major enzyme present in plants and microorganisms. Because the yeast *Saccharomyces* was one of the preferred materials in early biochemical studies, yeast invertase became one of the classical model enzymes. Mitscherlich described in 1842 the existence in yeast of a substance capable of inverting dextrorotatory cane sugar into a levorotatory sugar that was identified in 1847 by Dubrunfaut as a mixture of glucose and fructose. In 1860, for the first time, Berthelot carried out the isolation of invertase (see Ref. 1). Some years later, the whole theory of enzyme kinetics was based on experimental results obtained with yeast invertase (2). Because invertase was found to be intimately associated with the yeast cells and because its purification required the preparation of yeast extracts, it was considered to be an intracellular enzyme. However, de la Fuente and Sols (3) showed that the enzyme is secreted by yeast cells and that the hydrolysis of sucrose is extracellular. Subsequently, it was discovered that the yeast produces two types of invertase: a heavily glycosylated secreted form and a non-glycosylated intracellular form (4, 5). Yeast invertase is encoded by a family of repeated *SUC* genes (6–9). The enzyme is normally secreted by yeast as a heavily glycosylated octameric protein. The large mass of the protein leads to it being trapped in the cell wall (10, 11). Both the non-glycosylated cytoplasmic form and the secreted form of invertase are encoded by the same gene (8). These two forms are transcribed as two mRNAs of different length, which are translated into polypeptides of different size. In addition, the longer one encodes the signal peptide needed for secretion (12).

On the basis of sequence similarity, invertase is classified within family 32 of the glycoside hydrolases (13). In addition to invertases, this family (designated GH32) includes inulinases and levanases, involved in the hydrolysis of fructose-containing polysaccharides, and also transglycosylases with fructose transferase activity. GH32 enzymes act by a retaining mechanism in

* This work was supported in part by Grants BIO2010-20508-C04-02 and BIO2010-20508-C04-03 from the Spanish Ministry of Education and Science.
*The atomic coordinates and structure factors (code 4EQV) have been deposited in the Protein Data Bank (http://wwpdb.org/).*
[1] Both authors contributed equally to this work.
[2] Supported by a Junta para la Ampliación de Estudios (JAE) predoctoral fellowship from the Consejo Superior de Investigaciones Científicas.
[3] Present address: Instituto de Catálisis y Petroleoquímica, CSIC, E-28049 Madrid, Spain.
[4] To whom correspondence should be addressed. Tel.: 34-91-561-9400; Fax: 34-91-564-2431; E-mail: xjulia@iqfr.csic.es.

which an aspartate located close to the N terminus acts as the catalytic nucleophile and a glutamate acts as the general acid/base catalyst. The reaction proceeds through attachment of the aspartate nucleophile to a fructosyl unit of the donor substrate. The fructosyl is subsequently released by hydrolysis or transferred to an acceptor sugar substrate (transglycosylation). In recent years, the crystallographic structure of several GH32 enzymes from bacteria (14–16) and eukaryotes (17–21) have been reported. A close phylogenetic relative to *Saccharomyces* invertase (SInv)[5] is an inulinase from *Schwanniomyces occidentalis* (22). The characteristic structural feature of GH32 enzymes, shared by GH68 enzymes included in the same GH-J clan, is a 5-fold $\beta$-propeller catalytic domain consisting of five blades (each composed of four antiparallel $\beta$-strands with a "W" topology), which surround a central negatively charged active site cavity. The GH32 family differs from the GH68 family by an additional $\beta$-sandwich domain appended to the catalytic domain.

Besides its historical importance in the development of biochemistry, SInv has extensive industrial applications. It is one of the most widely used enzymes in confectionary to make liquid centers in candy making, and it is also used during fermentation of cane molasses into ethanol. A new potential application is the synthesis of prebiotic fructo-oligosaccharides used in functional foods and pharmaceutical formulations (23). The use of prebiotics to orchestrate the gut microbiota composition, with the associated benefit to human health, is an emerging issue of the utmost biotechnological interest (24).

In this work, we report the three-dimensional structure of SInv, produced in *Escherichia coli*, by expression of the *SUC2* coding sequence without the 5′-end of the gene corresponding to the secretion signal peptide. Our results reveal the structural basis of the unique oligomerization pattern observed in SInv and provide key factors to understanding the enzymatic activity and specificity of this important enzyme.

## EXPERIMENTAL PROCEDURES

*Cloning, Expression, and Purification*—The gene encoding SInv was expressed in *E. coli* Rosetta 2 cells carrying plasmid pQE-*SUC2*. The resulting His-tagged protein was purified by nickel affinity chromatography as described previously (23). For crystallization, the eluted fractions containing Suc2 (>95% purity according to SDS-PAGE analysis and Coomassie Blue staining) were dialyzed (1:10,000) against 0.05 M Tris-HCl buffer (pH 7) and concentrated using 20-kDa cutoff membrane ultrafiltration (Pierce). For activity assays, SInv was dialyzed (1:10,000) against 0.05 M phosphate buffer (pH 7) and 150 mM NaCl.

*Crystallization and Data Collection*—Crystallization of SInv (10 mg/ml in 0.05 M Tris-HCl (pH 7)) was performed on Cryschem sitting drop plates (Hampton Research) at 18 °C. Small bars grew in 3% PEG 3350, 5% 2-methyl-2,4-pentanediol, 0.6 M magnesium formate, 1 mM tris(2-carboxyethyl)phosphine, 0.33 M guanidinium chloride, and 0.1 Bistris (pH 6.5) (protein/precipitant drop ratio of 2:1) by vapor diffusion at room temperature. The crystals diffracted to 3.3 Å resolution. Many attempts to improve resolution at low temperature or using other techniques such as streak and microseeding or using agarose (2–3%) in the crystallization drops were unsuccessful. For more details about the crystallization behavior of this SInv, see Ref. 25.

Crystals of SInv belonged to space group $P3_121$, with eight molecules in the asymmetric unit and 75% solvent content within the unit cell. For data collection, native crystals were transferred to cryoprotectant solutions consisting of mother liquor plus 25% (v/v) glycerol before being cooled to 100 K in liquid nitrogen. Diffraction data were collected using synchrotron radiation at the European Synchrotron Radiation Facility (ESRF, Grenoble, France) on beamline ID23-1. Diffraction images were processed with iMOSFLM (26) and merged using the CCP4 package (27). A summary of data collection and data reduction statistics is provided in Table 1.

*Structure Solution and Refinement*—The structure of SInv was solved by molecular replacement using the MOLREP program (27). The structure of *S. occidentalis* $\beta$-fructofuranosidase (SoFfase; Protein Data Bank code 3KF3) was used to pre-

**TABLE 1**
**Crystallographic statistics of SInv**
Values in parentheses are for the high resolution shell. r.m.s.d., root mean square deviation.

| | |
|---|---|
| **Crystal data** | |
| Space group | $P3_121$ |
| Unit cell parameters (Å) | |
| *a* | 268.6 |
| *b* | 268.6 |
| *c* | 224.4 |
| **Data collection** | |
| ESRF Beamline | ID23-1 |
| Temperature (K) | 100 |
| Wavelength (Å) | 0.979 |
| Resolution (Å) | 56.31–3.30 (3.48–3.30) |
| **Data processing** | |
| Total reflections | 873,783 (134,865) |
| Unique reflections | 137,870 (17,424) |
| Multiplicity | 6.4 (5.0) |
| Completeness (%) | 98.5 (92.6) |
| Mean $I/\sigma(I)$ | 8.1 (2.0) |
| $R_{merge}$ (%)[a] | 20.5 (55.6) |
| $R_{pim}$ (%)[b] | 9.7 (37.7) |
| Molecules/asymmetric unit | 8 |
| Matthews coefficient (Å$^3$ Da$^{-1}$) | 24.9 |
| Solvent content (%) | 75 |
| **Refinement** | |
| $R_{work}/R_{free}$ (%)[c] | 22.2/23.9 |
| Mean *B*-factors | |
| Peptide | 51.2 |
| Water | 20.3 |
| No. of atoms | |
| Protein | 33,016 |
| Water molecules | 32 |
| Ramachandran (32) (%) | |
| Favored | 89.1 |
| Outliers | 2.5 |
| r.m.s.d. | |
| Bonds (Å) | 0.008 |
| Angles | 1.18° |
| Protein Data Bank code | 4EQV |

[a] $R_{merge} = \Sigma_{hkl}\Sigma_i|I_i(hkl) - (I(hkl))|/\Sigma_{hkl}\Sigma I_i(hkl)$, where $I_i(hkl)$ is the *i*th measurement of reflection *hkl*, and $(I(hkl))$ is the weighted mean of all measurements.
[b] $R_{pim} = \Sigma_{hkl}(1/(N-1))^{1/2}\Sigma_i|I_i(hkl) - (I(hkl))|/\Sigma_{hkl}\Sigma_i I_i(hkl)$, where *N* is the redundancy for the *hkl* reflection.
[c] $R_{work}/R_{free} = \Sigma_{hkl}|F_o - F_c|/\Sigma_{hkl}|F_o|$, where $F_c$ and $F_o$ are the calculated and observed structure factor amplitudes of reflection *hkl* for the working/free (5%) set, respectively.

[5] The abbreviations used are: SInv, *Saccharomyces* invertase; Bistris, 2-[bis(2-hydroxyethyl)amino]-2-(hydroxymethyl)propane-1,3-diol; SoFfase, *S. occidentalis* $\beta$-fructofuranosidase; NCS, non-crystallographic symmetry.

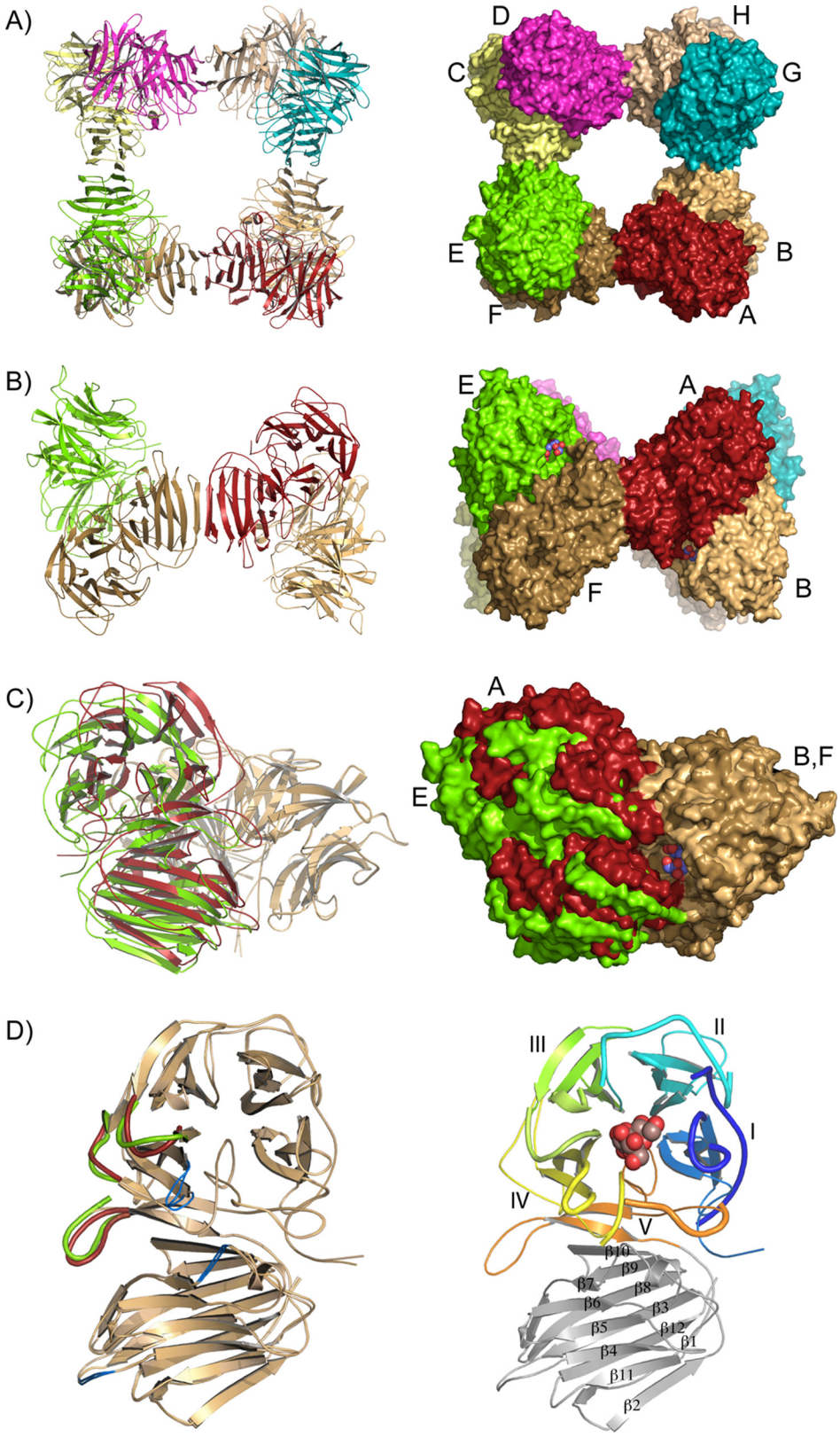


FIGURE 1. **Structure of octameric SInv.** *a*, view of the SInv octamer in ribbon (*left*) and solvent-accessible surface (*right*) representations, showing each subunit in a different color. In *b*, the octamer is rotated 90°, illustrating that it can be best described as a tetramer of two different kinds of dimers, AB/CD and EF/HG, which are compared by superimposing subunit F on subunit B in *c*. Then, a rotation of 15° would be necessary to bring out subunit E into the A position. Three regions of the polypeptide chain act as hinges (DynDom server), which are colored *blue* in *d* (*left*). The different dimer associations produce local conformational differences at the dimer interface in specific regions represented in *red* (A, B, C, and D) and green (E, F, G, and H). SInv folds into two domains, a catalytic $\beta$-propeller that is colored according to its five blades (I–V) and a C-terminal $\beta$-sandwich domain formed by two antiparallel six-stranded $\beta$-sheets (*right*). The putative position of a 1-kestose substrate molecule shown in *c* and *d* is inferred from structural superposition of SInv on the *Cichorium intybus* fructan 1-exohydrolase·1-kestose complex (Protein Data Bank code 2AEZ) to point out the active site cavity.

pare the search model with the program CHAINSAW (28) and a protein sequence alignment of SInv and SoFfase. A solution containing eight molecules in the asymmetric unit (molecules A–H) was found using reflections within the 50–3.5 Å resolution range and a Patterson radius of 45 Å, which, after rigid body fitting, led to an *R*-factor of 46%. Crystallographic refinement was performed using the program REFMAC (29) within the CCP4 suite with flat bulk solvent correction and using maximum likelihood target features. Tight local non-crystallographic symmetry (NCS) and jelly body restraints were applied during the first steps of refinement. The free *R*-factor was calculated using a subset of 5% randomly selected structure factor amplitudes that were excluded from automated refinement. Some regions of the polypeptide chain, in particular loops 190–200 and 230–240 and β-strand 228–250, all located at the interface between dimers, were not visible in the electron density of molecules EFGH and were excluded from the model during the first stages of the refinement. Furthermore, two NCS groups were defined composed of molecules ABCD and EFGH, respectively. After iterative refinement and rebuilding of these regions using the program Coot (30), the final $2F_o - F_c$ map showed continuous density for the whole protein. At the later stages, water molecules were included in the model, which, combined with more rounds of restrained refinement, led to a final *R*-factor of 22.9 ($R_{free}$ = 23.7) for all data set up to 3.3 Å resolution. Refinement parameters are reported in Table 1.

Stereochemistry of the models was checked with PROCHECK (31) and MolProbity (32). The figures were generated with PyMOL (33). Analysis of the interfacial surfaces and oligomer stability was done with the Protein Interfaces, Surfaces and Assemblies service (PISA) at the European Bioinformatics Institute (34). Root mean square deviation analysis was carried out with the program SUPERPOSE in the CCP4 package (27).

*Activity Assays*—Purified SInv was incubated for different times with sucrose, 1-kestose, nystose, raffinose, or inulin (from dahlia tubers) in 100 mM acetate buffer (pH 4.8) at 50 °C. The enzyme was inactivated by heating at 95 °C for 10 min. The calculation of the initial velocity of hydrolysis was based on the kinetics of product release. The products of the reaction were analyzed by anion exchange chromatography using a CarboPac PA100 column (4 × 250 mm) coupled to a pulsed amperometric detector (Dionex) as described previously (23).

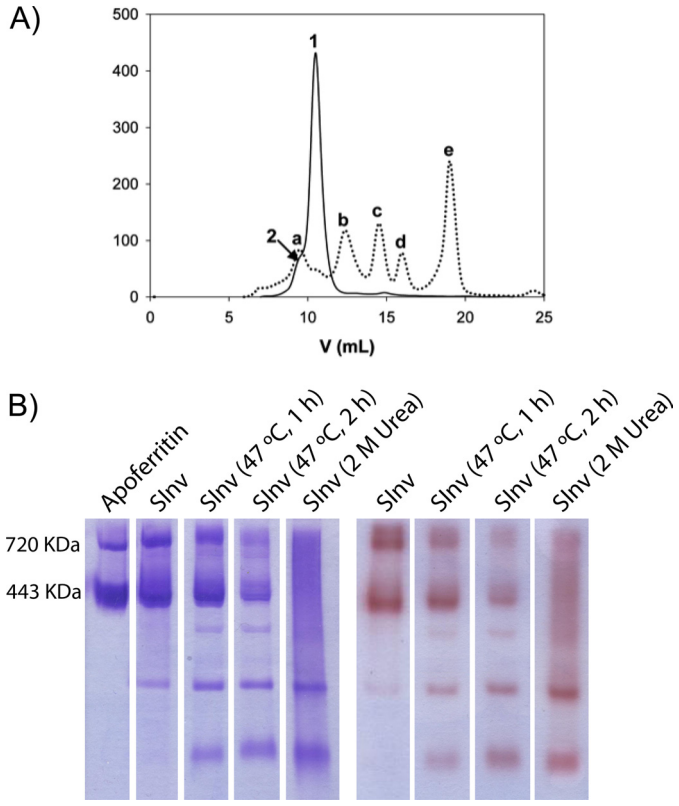


FIGURE 2. **Analysis of SInv oligomeric state.** *a*, size exclusion analysis of SInv. A sample of purified enzyme (2 mg/ml) in 0.05 M phosphate buffer (pH 7) and 150 mM NaCl was injected onto a Superdex 200 10/300 GL column coupled to an ÅKTA purifier system (GE Healthcare) previously equilibrated with the same buffer. Elution was carried out at a flow rate of 0.5 ml/min for 1.5 column volumes (*solid line*). SInv eluted mainly as a peak of ~430 kDa (*peak 1*), indicative of an octameric structure. A shoulder of this peak at lower elution volumes, highlighted with an *arrow* (*peak 2*), probably corresponds to higher molecular mass aggregates. Calibration of the column was performed with molecular mass standards (Bio-Rad catalog no. 151-1901) eluted under the same conditions (*dotted line*): *peak a*, thyroglobulin (670 kDa); *peak b*, γ-globulin (158 kDa); *peak c*, ovalbumin (44 kDa); *peak d*, myoglobin (17 kDa); and *peak e*, vitamin $B_{12}$ (1.35 kDa). *b*, nondenaturing PAGE analysis of purified SInv performed on 6% polyacrylamide gels. Gels were stained with Coomassie Blue (*left*), or alternatively, invertase activity was detected by incubating the gels in sucrose and subsequently staining with 1% (w/v) 2,3,5-triphenyltetrazolium chloride in 0.25 M NaOH (*right*) as described previously (22). Oligomers lower than the octamer appeared after heating SInv at 47 °C or incubating with urea. These treatments also decreased the proportion of the sample that formed higher aggregates. Other external conditions, such as addition of NaCl (0.1, 0.5, and 1 M), dilution (1:3, 1:5, and 1:10), or varying pH (4.5, 7.5, and 8.5), did not alter the pattern of untreated SInv (not shown).

## RESULTS

The invertase of the yeast *Saccharomyces* was produced in *E. coli*, purified, and crystallized as reported previously (25). We present here the three-dimensional structure of the enzyme solved by molecular replacement at 3.3 Å resolution. The experimental and structure determination details are given under "Experimental Procedures" and in Table 1. The crystals belong to space group $P3_121$, with the asymmetric unit containing a complete homo-oligomer of eight subunits. Each chain (A-B-C-D-E-F-G-H) consists of 512 residues with a molecular mass of 58.5 kDa as calculated from its primary structure. The imposition of tight NCS during early refinement led to a model with eight identical subunits. Most of the polypeptide chain exhibited good electron density, but there were some segments that remained undefined, mainly the regions located at the subunit interface. Consequently and according to the oligomerization pattern shown by SInv (described below), two strict NCS groups were defined so that chains A-B-C-D and E-F-G-H were refined independently. This scheme led to a continuous electron density in all the subunits, where all the residues could be fitted. The final model showed a root mean square deviation of 1.02 Å between respective Cα atoms from both NCS groups, with the differences being restricted to some particular regions of the polypeptide chain, as it will be explained below.

*Crystallized SInv Is an Octameric Enzyme*—The molecular mass of purified SInv, 428 kDa (see Fig. 2*b*), was consistent with an octamer association as proposed previously (25). Structural analysis showed that it is a flat square-shaped octamer with dimensions of 130 × 130 × 110 Å and is made up of eight subunits related by non-crystallographic 2-fold symmetry par-

**TABLE 2**
**Polar interactions at the SInv interfaces**
CD, SInv catalytic domain; βD, SInv β-sandwich domain. Asterisks indicate interactions at the active site pocket.

| Molecule B/D | | Molecule A/C |
|---|---|---|
| Hydrogen bonds | | |
| CD | | CD |
| GLN 171 (NE2) | * | GLU 323 (OE2) |
| ASN 194 (ND2) | | ASP 254 (OD1) |
| ASN 255 (ND2) | | GLU 195 (OE1) |
| SER 257 (OG) | | SER 257 (OG) |
| ASN 321 (ND2) | * | GLN 171 (O) |
| ASN 321 (ND2) | * | TYR 200 (O) |
| THR 324 (OG1) | * | GLN 171 (O) |
| CD | | βD |
| GLY 235 (N) | * | SER 439 (OG) |
| βD | | βD |
| ARG 406 (NH1) | | GLU 430 (O) |
| GLU 410 (N) | * | TYR 433 (OH) |
| TYR 433 (OH) | | SER 415 (O) |
| THR 435 (OG1) | | ARG 437 (O) |
| ASN 436 (N) | | ASN 436 (OD1) |
| ARG 437 (NH1) | | PHE 434 (O) |
| ARG 437 (NH1) | | VAL 428 (O) |
| PHE 434[ O ) | | ARG 437[ NH1] |
| **Molecule F/H** | | **Molecule E/G** |
| Hydrogen bonds | | |
| βD | | βD |
| ARG 406 (NH1) | | GLU 430 (O) |
| SER 415 (OG) | | TYR 433 (OH) |
| TYR 433 (OH) | * | SER 415 (O) |
| TYR 433 (OH) | * | SER 415 (OG) |
| ARG 437 (NE) | * | ASN 436 (OD1) |
| ARG 437 (NE) | | PHE 434 (O) |
| ARG 437 (NH1) | | LYS 429 (O) |
| ARG 437 (NH2) | * | ASN 436 (OD1) |
| Salt bridges | | |
| CD | | βD |
| ASP 45 (OD2) | * | LYS 385 (NZ) |
| **Molecule F/G/E/H** | | **Molecule A/B/C/D** |
| Hydrogen bonds | | |
| βD | | βD |
| ARG 345 (N) | | TYR 358 (OH) |
| ARG 345 (NE) | | THR 348 (O) |
| THR 348 (OG1) | | THR 348 (OG1) |
| THR 350 (OG1) | | TRP 343 (O) |
| SER 357 (N) | | ASP 361 (O) |
| ASN 359 (N) | | ASN 359 (O) |
| ASP 361 (N) | | SER 357 (O) |
| SER 363 (N) | | ALA 355 (O) |
| ALA 355 (O) | | SER 363 (N) |
| SER 357 (O) | | ASP 361 (N) |
| ASN 359 (O) | | ASN 359 (N) |
| ASP 361 (O) | | SER 357 (N) |

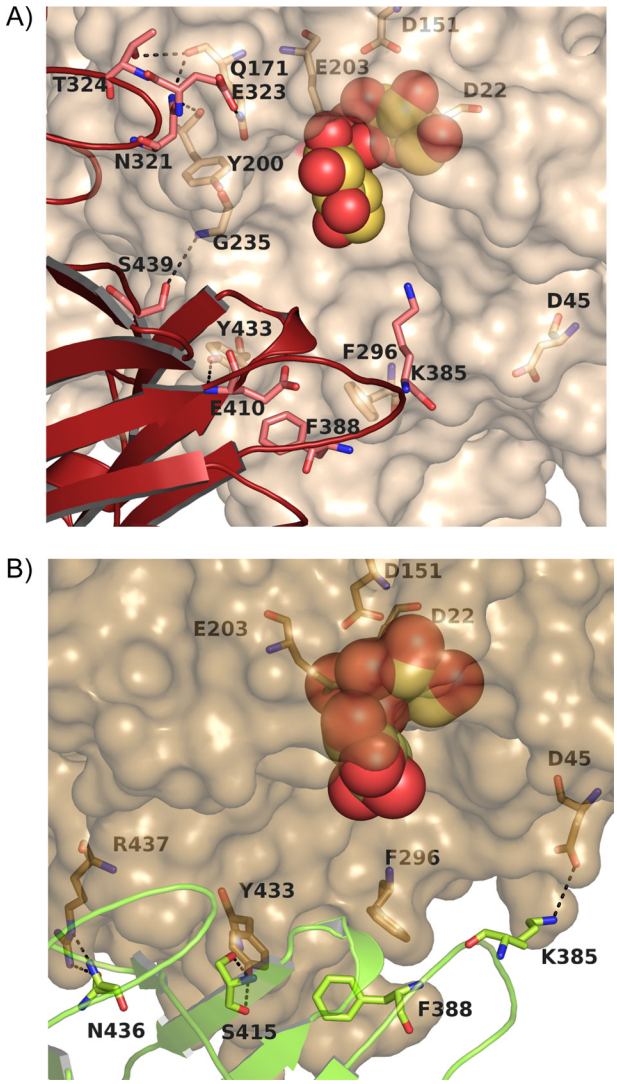


FIGURE 3. **Dimer interface at the active site.** The octameric SInv active site interfaces are detailed, keeping the same color pattern in Fig. 1*c*, with one subunit being shown in ribbon representation for clarity. *a*, the AB/CD dimers are tightly made by interactions among both their catalytic and β-sandwich domains. The base of the catalytic pocket is additionally lined by hydrophobic interactions through Phe-388 and Phe-296. *b*, by contrast, the EF/GH dimers interact only through their β-sandwich domains. In addition, the catalytic pocket is also paved by a new salt bridge formed between Asp-45 and Lys-385 from the β-sandwich domain, which lines the cavity. A putative 1-kestose molecule is shown in spherical representation (inferred as explained in the legend to Fig. 1).

allel to the *c* axis in a 222 arrangement (Fig. 1*a*). Its molecular surface is 136,914 Å$^2$, with a total buried surface area of 22,296 Å$^2$.

However, this octamer is best described as a tetramer of dimers that oligomerize by intersubunit extension of the two β-sheets that end the β-sandwich domain within each subunit (Fig. 1*b*). Furthermore, close inspection revealed that SInv forms two classes of dimers, AB/CD and EF/GH, which are located at opposite vertices of the square. The subunits of these two classes of dimers associate differently with each other, and, thus, the EF/GH dimers can be described as an "open" assembly, whereas the AB/CD dimers form a "closed" arrangement. Structural superposition of chain B on chain F shows that a 15° rotation would be necessary to bring monomer A into the E

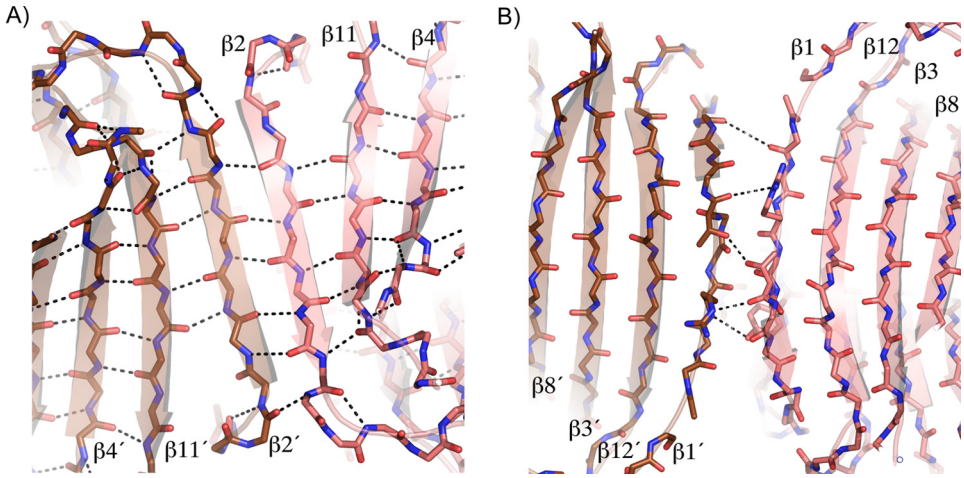


FIGURE 4. **Intermolecular *β*-sheet.** Both sets of dimers assemble through a similar interface that involves the extension of their corresponding *β*-sheets between each *β*-sandwich domain. *a*, view of the internal part at the octamer interface showing that the hydrogen bond pattern centered on *β*2 corresponds to a regular *β*-sheet. *b*, in contrast, the external wall is defined by polar links between the side chains of the residues at *β*1.

position (Fig. 1*c*), with three regions of the SInv monomer acting as hinges (colored *blue* in Fig. 1*d*, *left*).

On the other hand and like the known GH32 members, the SInv subunit folds into two domains, a catalytic *β*-propeller domain (residues 1–334) and a *β*-sandwich domain (residues 342–512), linked by a short loop (Fig. 1*d*, *right*). In turn, the *β*-propeller domain is assembled from five blades (I–V), each consisting of four antiparallel *β*-strands (A–D, from the axis toward the outside of the propeller) connected by turns in a classical W pattern. Blade I is the most and blade IV is the least conserved among GH32 family members. The catalytic site is located at the axis of the propeller and is shaped by the loops connecting the different blades (L1–L4) and the turns linking strand B to strand C within each blade (TI–TV). On the other hand, the *β*-sheet domain has two six-stranded antiparallel *β*-sheets folded into a *β*-sandwich topology and is the region presenting the lowest sequence homology among GH32 family members.

The quaternary structure of SInv in solution has been analyzed by different methods. Recombinant SInv subjected to gel filtration chromatography eluted mainly as a peak corresponding to the size of an octamer, although a small fraction of the protein appeared as aggregates of higher molecular mass (Fig. 2*a*). This tendency to aggregate was also observed on nondenaturing polyacrylamide gels (Fig. 2*b*). Oligomers of less than eight units (hexamers, tetramers, and dimers) were also detected, and incubation of the enzyme at 47 °C for 1–2 h or treatment with 2 M urea stimulated the dissociation of the octameric form. The enzyme was active in all these different oligomerization states, as shown by the zymogram test (Fig. 2*b*). Variability in quaternary structure was also observed by ultracentrifuge analysis (data not shown), which indicated that SInv was octameric but showed a decrease in the average molecular mass at the highest centrifugation force (11,000 rpm). These results are in good agreement with those reported for both intracellular and secreted forms of the native enzyme (10, 35).

*Different Atomic Interactions Define Dimer Association*—Table 2 lists the polar interactions found within each interface of the octamer. First, the AB/CD dimers are tightly associated by interactions among both their catalytic and *β*-sandwich domains (Fig. 1*c*). Fourteen of a total of 32 hydrogen bonds are made between their catalytic domains, mainly through loop L3 and strand D4 and also through a long loop connecting strands C5–D5 (residues 316–328) that makes many interactions near the catalytic pocket, as shown in Fig. 3*a*. Furthermore, the catalytic pocket of one monomer is surrounded by loops from the *β*-sandwich domain of the other, and there is a polar interaction from Ser-439 to Gly-235 located at TIV that stabilizes the dimer interface at this region. The base of the catalytic pocket is additionally lined by hydrophobic interactions through Phe-388 and Phe-296 (TV) and direct polar interaction between both *β*-sandwich domains (Table 2).

By contrast, the EF/GH dimers lack atomic interactions between their catalytic domains, as shown in Table 2, and keep only some hydrogen links between their *β*-sandwich domains, with half of them not being conserved with respect to the closed dimers. However, the catalytic pocket is also strengthened by a new salt bridge formed between Asp-45 (at loop TI) and Lys-385 (at the loop linking *β*3–*β*4 of the *β*-sandwich domain), which encloses a well defined cavity (Fig. 3*b*). This different pattern of interaction between the subunits of the two kinds of dimers has two direct implications. First, the EF/GH active site has a wider pocket (Fig. 1*c*). Second, the lack of interactions between the catalytic domains produces a rearrangement in the dimer interface regions that leads to the structural differences of the two kinds of dimers (Fig. 1*d*).

Both types of dimers assemble through a similar interface that involves the extension of the two *β*-sheets of each *β*-sandwich domain (Fig. 4) centered on *β*1 and *β*2, respectively. It is interesting that the sheet constituting the "inner" part of the octamer (Fig. 4*a*) forms a regular antiparallel intermolecular *β*-sheet, similar to that reported in multimeric lectins, cytokines, and other proteins (36). These intermolecular interactions between the hydrogen-bonding edges of *β*-sheets are considered to be a fundamental form of biomolecular recognition (like DNA base pairing) and are involved not only in oligomerization and protein-protein interactions but also in protein aggregation, as they occur in *β*-amyloid fibril formation (37).

**TABLE 3**
**Analysis of the interfaces**

| Assembly | Interface area | $\Delta^iG$ | $\Delta^iG$ *p* value | $N_{HB}$ | $N_{SB}$ | $N_{DS}$ |
|---|---|---|---|---|---|---|
| | *Å²* | *kcal/mol* | | | | |
| AB/CD | 2664.1 | −20.9 | 0.035 | 30 | 0 | 0 |
| EF/GH | 1376.2 | −5.5 | 0.352 | 17 | 2 | 0 |
| CE/AF/DH/BG | 767.4 | −2.4 | 0.431 | 12 | 0 | 0 |

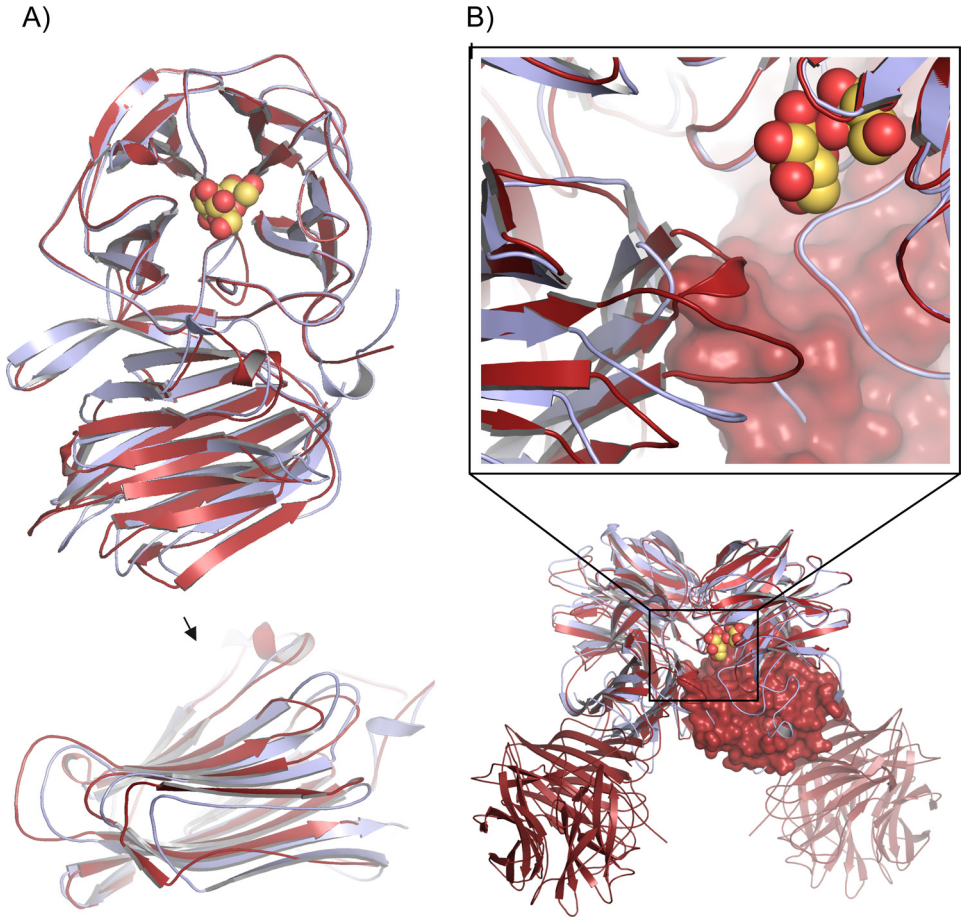


FIGURE 5. **Structural differences between SInv and SoFfase.** *a*, structural alignment of the SoFfase subunit (*slate*) and the SInv monomer (*red*) shows well conserved catalytic domains but larger differences in the β-sandwich domain, mostly at strands β1 and β2, at the base of the β-sandwich domain, which can be attributed to the interactions of the β-sandwich elements in the SInv octamer. *b*, the β-sandwich of an SInv subunit is shown in surface representation to highlight the effect of the different arrangement in the active site (magnified) at the dimer interface. The putative 1-kestose position is shown in spherical representation (inferred as explained in the legend to Fig. 1).

Table 3 summarizes the main features of the different interfaces found in the octamer as analyzed by the PISA program (34). As shown, the interface area of the closed dimers is twice that found in the open dimers, as is the number of polar interactions. The binding energy ($\Delta^iG$) is negative in all interfaces, indicating their hydrophobic nature, but the *p* value reveals that the AB/CD interfaces, with lowest $\Delta^iG$, have a large hydrophobicity at a higher confidence level. Therefore, only the closed dimers, AB/CD, might be expected to exist in solution. The other interfaces may represent weak interactions (38) existing in higher oligomers of SInv depending on external conditions. This agrees with the oligomerization behavior of both cytosolic and secreted SInv isoforms (10, 35).

*A Few Changes in Its Sequence Determine the Oligomerization Pattern of SInv*—The specific role of the β-sandwich domain in GH32 enzyme functionality remained elusive for a long time. The first experimental evidence of its implication in dimerization and substrate binding became available when the first structure from a yeast enzyme, SoFfase, was reported (22). Very recently, the unique role of its β-sandwich domain in substrate recognition has been further demonstrated from the structure of two complexes with long substrates (39). Although SoFfase and SInv share 68% sequence homology (being 48% identical), SoFfase is a dimeric enzyme, and higher aggregation forms have not been detected.

Structural superimposition of SInv and SoFfase (Fig. 5) revealed that the catalytic domains are almost identical and that most regions of the β-sandwich domain are very similar. Accordingly, the hydrogen link pattern in the SoFfase dimer is very similar to that in the closed AB/CD SInv dimers. However, it is remarkable that none of the residues that provide the polar links for the β-sheet extension through β1 and β2 are conserved in SoFfase. Consequently, this region shows poor structural alignment (Fig. 5). Furthermore, the β1–β2 region in

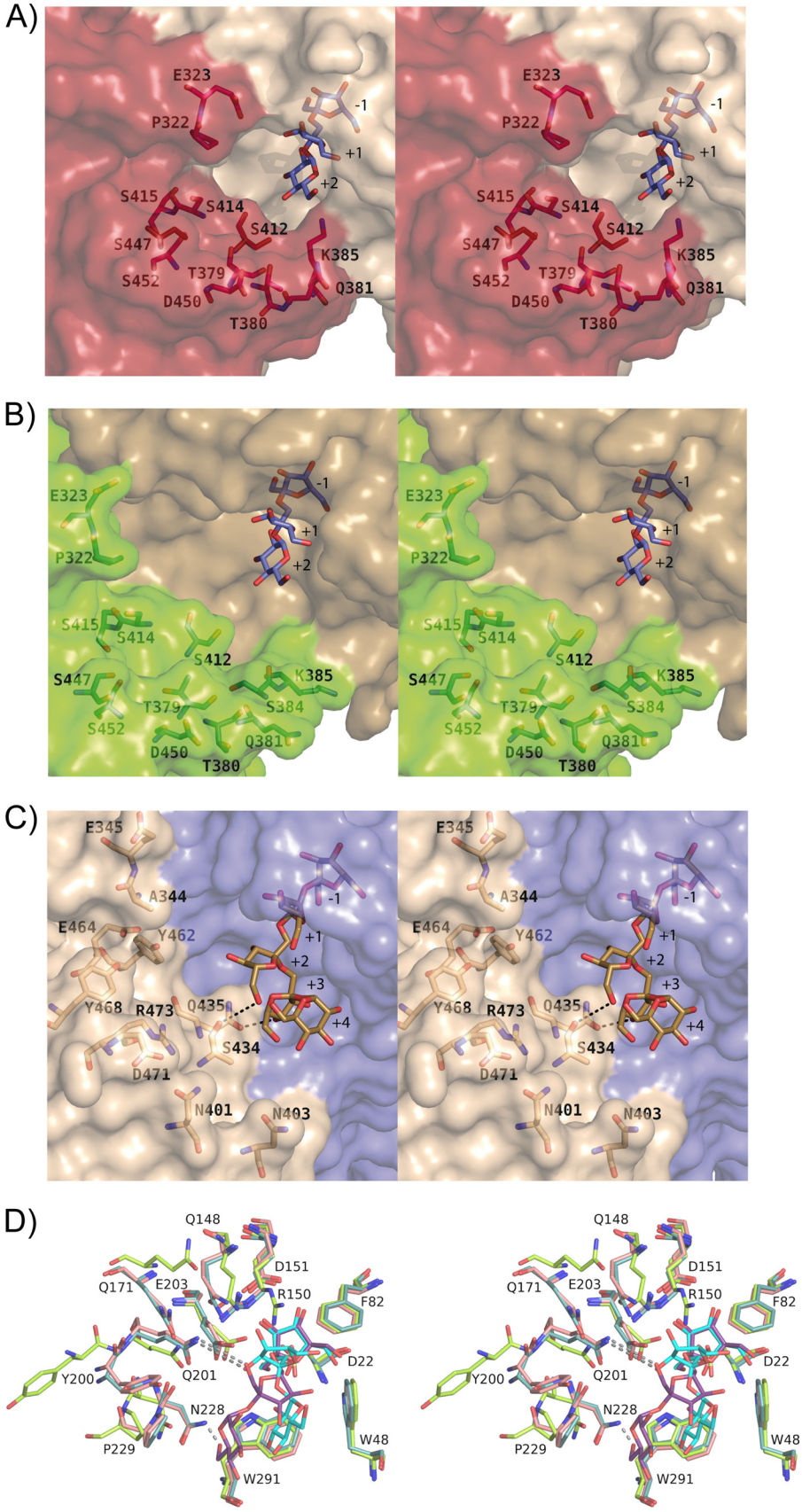

SoFfase has a high content of Lys residues (9/20), which are solvent-exposed at the base of the β-sandwich, yielding a positively charged surface that would prevent dimer association along this region due to electrostatic repulsion effects.

*Quaternary Structure Determines Substrate Specificity*—The active site of SInv is located at the interface within each pair of dimers. Because of the two different ways subunits can form dimers (Fig. 1*c*), the active sites in these dimers may have different environments. Thus, the AB/CD dimers form a very narrow pocket of 10 × 10 Å that seems unable to accommodate an oligosaccharide with more than three or four sugar units (Fig. 6*a*). In contrast, the wider (20 × 16 Å) entrance cavity observed in the EF/GH dimers might allow longer substrates (Fig. 6*b*), although this could involve a significant, energetically expensive distortion of the polysaccharide.

A comparison of the catalytic pockets of octameric SInv and SoFfase (Fig. 6*c*) reveals that the shape and size of the SoFfase cavity is more similar to those within the open EF/GH SInv dimers. Nevertheless and more significant, the chemical nature of the residues that form the β-sandwich domain surrounding the active center is quite different in the two enzymes. SoFfase has long chain residues, such as Arg-473, Glu-464, Tyr-462, and Tyr-468 and notably Gln-435, a residue that, together with Ser-412, makes direct polar links with the oligosaccharides at subsite +3 (Ref/ 39 and nomenclature according to Ref. 40). Furthermore, Asn-401, Asn-403, and Asp-471 protrude at the entrance of the slot and define the polar boundaries that make accessible the cavity from the solvent. Therefore, most of the relevant SoFfase residues are highly flexible. By contrast, most of the corresponding SInv residues are short chain amino acids, such as Ser-412, Ser-414, Ser-415, Thr-379, Thr-380, and Ser-447. Consequently, the SoFfase active site seems more flexible to accommodate long chain substrates compared with the two catalytic pockets of SInv. This feature may therefore illustrate the structural basis for the activity of SInv as an invertase, whereas SoFfase is in fact an inulinase. As observed when comparing the activity of SInv with different oligosaccharides, the highest efficiency was with sucrose as a substrate, followed by the trisaccharides raffinose and 1-kestose, whereas the tetrasaccharide nystose was hydrolyzed at a much lower rate (Table 4). SInv showed no significant activity with inulin as the substrate.

It has been reported that SInv and SoFfase have some degree of transglycosylating activity, giving 6-kestose as the main product. This activity can be enhanced by mutagenesis (23, 39, 41). In contrast, homologous plant enzymes of the same GH32 family yield mostly 1-kestose. To understand the β(2,6) or β(2,1) nature of the transglycosylation reaction, the binding site on the putative acceptor sucrose and its orientation relative to the fructose unit in the covalent intermediate must be identified. Fig. 6*d* illustrates a superimposition of SInv and SoFfase catalytic pockets showing the putative position of the products 1-kestose and 6-kestose. The figure suggests that the nucleophile (Asp-22 in SInv numbering) environment, together with the hydrophobic wall of the pocket (Trp-48, Phe-82, and Trp-291), is coincident in all three cavities. Gln-201 is well positioned to make polar links with the fructose unit at subsite +1 in both transfructosylating products, Asn-228 could link to the glucose moiety of 6-kestose, and the glucose term of 1-kestose would stack with Trp-48. An essential role is thus assigned to Gln-201 to facilitate the transfructosylation reaction by binding the acceptor sucrose, whereas Asn-228 would crucially determine the product specificity as predicted (23) and also as described for SoFfase (39).

**TABLE 4**
**Activity of SInv**

| Substrate | Activity |
|---|---|
| | *μmol/min/mg* |
| Sucrose | 520 ± 20[a] |
| 1-Kestose | 102 ± 11[a] |
| Nystose | 36 ± 1[a] |
| Raffinose | 187 ± 8[a] |
| Inulin | 2.5 ± 0.1[b] |

[a] The substrate concentration was 250 mM.
[b] The substrate concentration was 10%.

In summary, the architecture of the active site, as determined by the way the enzyme monomers are assembled, explains both substrate specificity for hydrolysis (invertase *versus* inulinase activity) and transfructosylation product specificity. Thus, the dimerization mode of SInv modulates its hydrolytic activity, precluding the recognition of long chain substrates. This is more apparent for the closed dimers that would be predominant in aggregation states lower than the octamer or in alternative octameric forms composed exclusively of closed dimers (see "Discussion"). However, the transfructosylating mechanism would be the same in both enzymes.

## DISCUSSION

The yeast *Saccharomyces* plays an outstanding role in human civilization as the fermentative agent that produces bread, wine, and beer. *Saccharomyces* owes its predominant position as a fermentative microorganism to a very successful metabolic strategy. In the sugar-rich ecological niches where it dwells, *Saccharomyces* performs a highly efficient mobilization of sugars, which can be channeled to the production of an antiseptic substance (ethanol) that avoids the proliferation of competing microorganisms instead of being used for the production of biomass. The function of a set of enzymes involved in sugar metabolism, including invertase, is critical for the prevalence of *Saccharomyces* in its natural habitat. Despite the important

FIGURE 6. **Specificity of SInv.** Shown are stereo views of the SInv active site of the AB/CD (*a*) and EF/GH (*b*) dimers compared with the SoFfase dimer (*c*). The putative position of the substrate 1-kestose (inferred as explained in the legend to Fig. 1) is shown in *a* and *b*. A fructosylnystose molecule (*beige*) found in the reported E230A SoFfase complex (Protein Data Bank code 3U75) shown in *c* could enter into the EF/GH active site pocket (*b*), whereas the narrow entrance at the AB/CD interface (*a*) would prevent binding of extended fructans. Moreover, in SInv, the short chain residues surrounding the cavity outline a more rigid and therefore less flexible active site to accommodate long and polymeric oligosaccharides. *d*, structural alignment of SoFfase (*slate*) in the SInv catalytic pockets (ABCD (*red*) and EFGH (*green*)) showing the nucleophile (Asp-22), the intermediate stabilizer (Asp-151), and the acid/base catalyst (Glu-203). The putative positions of the transfructosylation products 1-kestose and 6-kestose are shown in *cyan* and *purple*, respectively. The position of 6-kestose has been inferred from superposition of its coordinates extracted from the Cambridge Structural Database (CSD; refcode CELGIC) onto the fructose of docked 1-kestose at subsite −1. The recognition scheme of the donor sucrose moiety giving each product within the AB/CD dimers would be the same as that described for SoFfase, as explained under "Results."

physiological role of SInv and its historical relevance as a model enzyme in early biochemical studies (2), its crystallographic structure had not yet been reported. Although it is secreted by the yeast in large amounts, native SInv appears as a heavy hyperglycosylated protein of heterogeneous molecular mass, which remains trapped in the cell wall (10). It is therefore a rather unsuitable material for crystallization. The biosynthesis and secretion of extracellular proteins by eukaryotes are a complex process in which transit of the nascent polypeptide through the endoplasmic reticulum is coupled with core glycosylation and protein folding. Hyperglycosylation takes place at a later stage in the Golgi and does not affect SInv folding or catalytic activity (42). Due to the fact that core glycosylation is often a necessary condition for proper protein folding, secreted eukaryotic proteins cannot be functionally expressed in *E. coli*. Therefore, the collection of a sufficient amount of protein for crystallization analysis requires either that it is abundantly produced by the organism from which derives or that it is heterologously expressed in a eukaryotic host. Examples of structurally determined SInv homologs of the GH32 family are therefore fungal inulinases abundantly produced by their natural host (17, 20, 22), plant fructosylases heterologously expressed in *Pichia pastoris* (18, 19), and a plant fructosyltransferase abundant in leaves (21). *Saccharomyces* produces an intracellular non-glycosylated version of the invertase (4). The intracellular version, which is synthesized as a soluble protein, is encoded by the same gene as the secreted form (12). Secondary and tertiary structures of both forms are virtually identical, as revealed by CD spectroscopy analysis (35). These considerations led us to carry out heterologous expression of SInv in

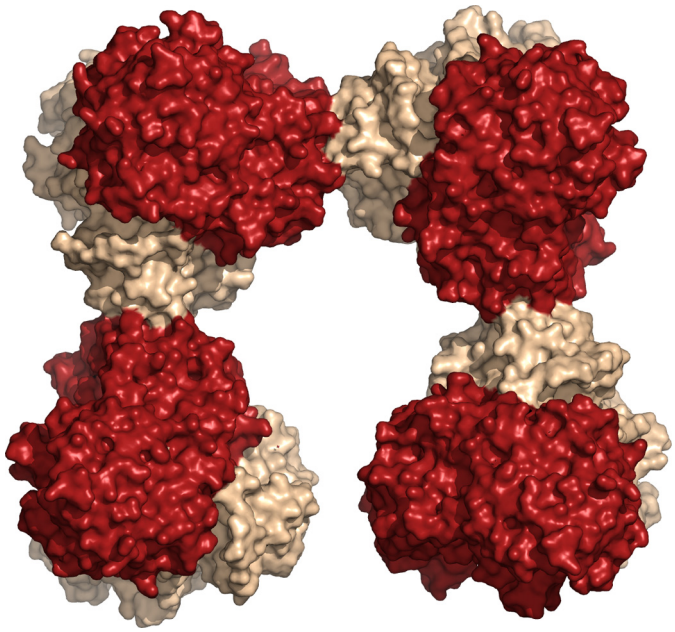

FIGURE 7. **Model of extracellular SInv.** Shown is a putative model of secreted octameric SInv built manually from the AB dimers, with retention of the intermolecular β-sheet. This model reproduces the electron micrographs reported for this isoform (10, 11), which showed rectangles slightly open in one side.

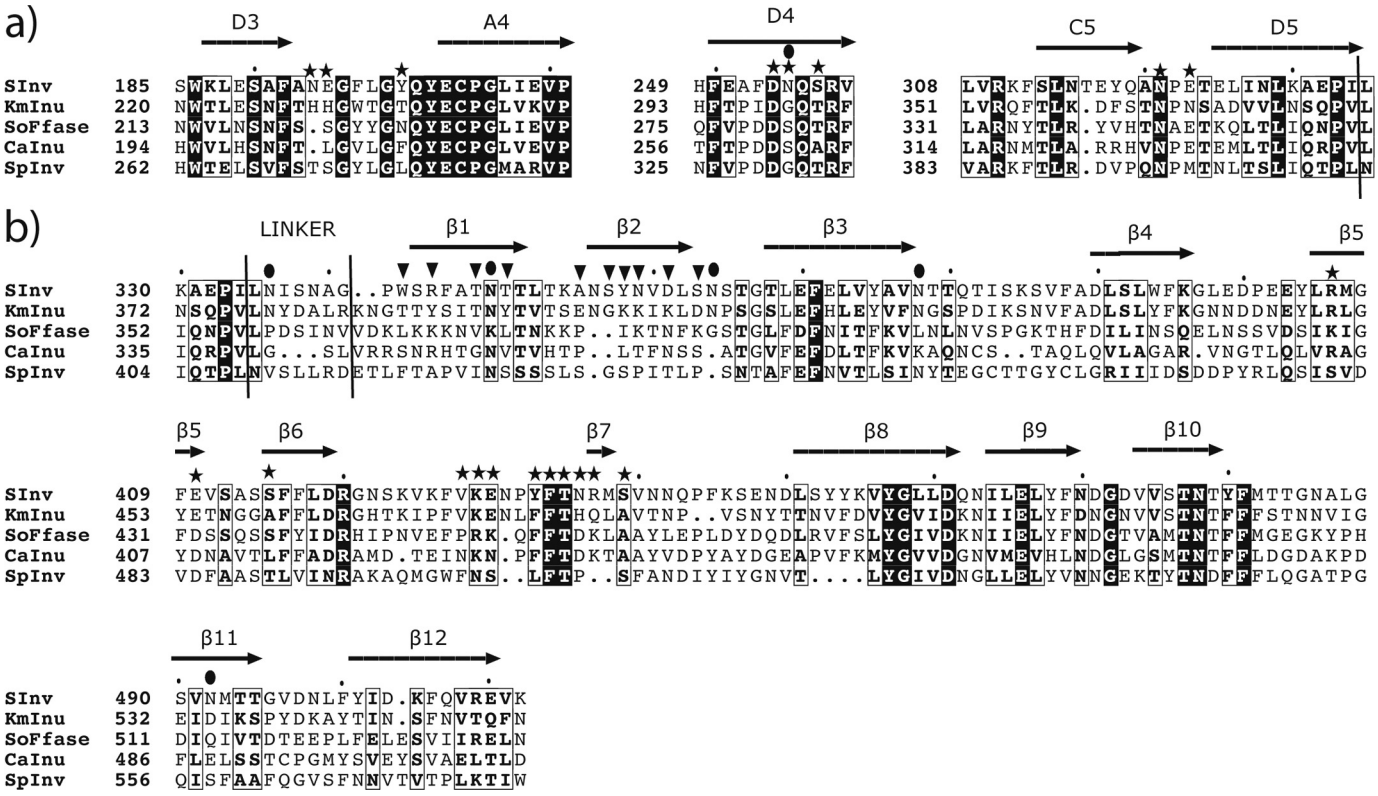


FIGURE 8. **Sequence conservation within GH32 family members from yeast.** The SInv sequence is aligned with other yeast enzymes: *Kluyveromyces marxianus* inulinase (*KmInu*), SoFfase, *Candida* sp KRF1 inulinase (*CaInu*), and *Schizosaccharomyces pombe* invertase (*SpInv*). Conserved regions are *highlighted* (44). The regions of the catalytic domain involved in making the dimer interface are shown in *a*, whereas the β-sandwich domain is shown in *b*. *Stars* specify residues involved in polar links within the AB/CD dimer interface. *Inverted triangles* indicate residues that make polar links between the β-sandwich domains from contiguous subunits responsible for the formation of the intermolecular β-sheets. *Solid circles* are potential *N*-glycosylation sites in extracellular SInv.

*E. coli*, which yielded suitable protein material for crystallization analysis (25).

Analysis of the crystal structure at 3.3 Å resolution that we have reported here showed that SInv folds into the catalytic β-propeller and β-sandwich domains characteristic of GH32 enzymes. A dimer association that shapes the active site has been found, similarly to that described in the phylogenetically close β-fructosidase from *S. occidentalis* (22). However, in contrast, SInv displays a special assembly of dimers into octamers through extension of each subunit β-sandwich domain. The particular geometry of the octamer generates closed and open dimers that are located alternatively at the vertices of a rectangle. Analysis of the interfaces and binding energy calculation showed that "closed-type" dimers are more stable. Although the octameric form is predominant in a fresh preparation of the enzyme (Fig. 2*a*), the weaker association within the "opened-type" dimer and the dimer-dimer interface may explain the instability manifested by the octamer upon incubation at higher (47 °C) temperatures (Fig. 2*b*) or at a high centrifugal force. Consequentially, recombinant SInv is predominantly an octamer but may exist as a dimer and other oligomeric forms, as has been reported for both the cytosolic and secreted isoforms (10, 11, 35, 43). Furthermore, as seen from the structure reported here, SInv dimerization plays a determinant role in substrate specificity, preventing binding of extended substrates, which explains its invertase character at the molecular level.

Electron micrographs of both internal and secreted SInv (10, 11) show a similar association pattern of spherical units with different oligomerization states: dimers, tetramers, hexamers, and octamers. Interestingly, secreted SInv octamers appear slightly open to one side, whereas intracellular invertase octamers appear mostly as nearly symmetrical closed rectangles, like the structure presented here. The electron micrographs of secreted invertase octamers resemble strikingly the model illustrated in Fig. 7, in which the protein would be composed of closed dimers linked by intermolecular β-sheets.

Although GH32 enzymes are generally highly conserved in the β-propeller and less so in the β-sandwich domain, SInv and SoFfase are very similar also in some regions of the β-sandwich domain, namely strands β8–β10 and region β6–β7. However, strands β1 and β2, which build the intermolecular β-sheet within the octamer, are less conserved. In fact, homology alignments of yeast GH32 sequences show that many of them contain a Pro residue at β1 or β2 that probably precludes intermolecular β-sheet formation (Fig. 8). In SoFfase, an unusually large number of solvent-exposed Lys residues are found in this region, resulting in a positively charged surface that likely interferes with β-sheet dimerization because of electrostatic repulsion effects. Therefore, the association of dimers into octamers seems to be a unique SInv feature.

To conclude, the structure of SInv presented here is an interesting new example of how non-catalytic domains with, unknown function play a role in fine-tuning enzymatic function. The contribution of the β-sandwich domain in building the catalytic pocket of GH32 yeast enzymes has been reported previously. However, a role in higher oligomerization leading to new specificity seems unique to SInv. The production of a complex octameric hyperglycosylated enzyme precludes its diffusion outside the periplasmic space. The secretion of invertase that occurs in many microorganisms represents an evolutionary advantage eliminating a mechanism for sucrose import. The unique quality of *Saccharomyces* is that it keeps the invertase trapped on the cell surface, avoiding its diffusion into the medium, where it would also aid competing organisms. We hope that the resolution of the sophisticated molecular architecture of this enzyme may contribute to the understanding of protein-carbohydrate interactions and to the design of novel, more efficient enzymes for biotechnological purposes.

*Acknowledgments—We thank the staff of the European Synchrotron Radiation Facility for providing beam time and for technical assistance at beamline ID23-1. We also thank Simon P. Gough for kindly reviewing the manuscript.*

## REFERENCES

1. Barnett, J. A. (2003) Beginnings of microbiology and biochemistry: the contribution of yeast research. *Microbiology* **149,** 557–567
2. Michaelis, L., and Menten, M. L. (1913) The Kinetics of Invertase Action. *Biochem. Z.* **49,** 333–369
3. de la Fuente, G., and Sols, A. (1962) Transport of sugars in yeasts. II. Mechanisms of utilization of disaccharides and related glycosides. *Biochim. Biophys. Acta* **56,** 49–62
4. Gascón, S., and Lampen, J. O. (1968) Purification of the internal invertase of yeast. *J. Biol. Chem.* **243,** 1567–1572
5. Gascón, S., Neumann, N. P., and Lampen, J. O. (1968) Comparative study of the properties of the purified internal and external invertases from yeast. *J. Biol. Chem.* **243,** 1573–1577
6. Gilliland, R. B. (1949) A yeast hybrid heterozygotic in four fermentation characters. *Compt Rend. Trav. Lab. Carlsberg Ser. Physiol.* **24,** 347–356
7. Winge, O., and Roberts, C. (1952) The relation between the polymeric genes for maltose, raffinose, and sucrose fermentation in yeasts. *Compt. Rend. Trav. Lab. Carlsberg Ser. Physiol.* **25,** 141–171
8. Grossmann, M. K., and Zimmermann, F. K. (1979) The structural genes of internal invertases in *Saccharomyces cerevisiae*. *Mol. Gen. Genet.* **175,** 223–229
9. Carlson, M., Osmond, B. C., and Botstein, D. (1981) *SUC* genes of yeast: a dispersed gene family. *Cold Spring Harb. Symp. Quant. Biol.* **45,** 799–803
10. Esmon, P. C., Esmon, B. E., Schauer, I. E., Taylor, A., and Schekman, R. (1987) Structure, assembly and secretion of octameric invertase. *J. Biol. Chem.* **262,** 4387–4394
11. Tammi, M., Ballou, L., Taylor, A., and Ballou, C. E. (1987) Effect of glycosylation on yeast oligomer stability. *J. Biol. Chem.* **262,** 4395–4401
12. Perlman, D., and Halvorson, H. O. (1981) Distinct repressible mRNAs for cytoplasmic and secreted yeast invertase are encoded by a single gene. *Cell* **25,** 525–536
13. Cantarel, B. L., Coutinho, P. M., Rancurel, C., Bernard, T., Lombard, V., and Henrissat, B. (2009) The Carbohydrate-Active EnZymes database (CAZy): an expert resource for glycogenomics. *Nucleic Acids Res.* **37,** D233–D238
14. Alberto, F., Bignon, C., Sulzenbacher, G., Henrissat, B., and Czjzek, M. (2004) The three-dimensional structure of invertase (β-fructosidase) from *Thermotoga maritima* reveals a bimodular arrangement and an evolutionary relationship between retaining and inverting glycosidases. *J. Biol. Chem.* **279,** 18903–18910
15. Bujacz, A., Jedrzejczak-Krzepkowska, M., Bielecki, S., Redzynia, I., and Bujacz, G. (2011) Crystal structures of the apo form of β-fructofuranosidase from *Bifidobacterium longum* and its complex with fructose. *FEBS J.* **278,** 1728–1744
16. Park, J., Kim, M. I., Park, Y. D., Shin, I., Cha, J., Kim, C. H., and Rhee, S. (2012) Structural and functional basis for substrate specificity and catalysis of levan fructotransferase. *J. Biol. Chem.* **287,** 31233–31241
17. Nagem, R. A. P., Rojas, A. L., Golubev, A. M., Korneeva, O. S., Eneyskaya,

E. V., Kulminskaya, A. A., Neustroev, K. N., and Polikarpov, I. (2004) Crystal structure of exo-inulinase from *Aspergillus awamori*: the enzyme fold and structural determinants of substrate recognition. *J. Mol. Biol.* **344,** 471–480
18. Verhaest, M., Van den Ende, W., Roy, K. L., De Ranter, C. J., Laere, A. V., and Rabijns, A. (2005) X-ray diffraction structure of a plant glycosyl hydrolase family 32 protein: fructan 1-exohydrolase IIa of *Cichorium intybus*. *Plant J.* **41,** 400–411
19. Verhaest, M., Lammens, W., Le Roy, K., De Coninck, B., De Ranter, C. J., Van Laere, A., Van den Ende, W., and Rabijns, A. (2006) X-ray diffraction structure of a cell-wall invertase from *Arabidopsis thaliana*. *Acta Crystallogr. D* **62,** 1555–1563
20. Pouyez, J., Mayard, A., Vandamme, A. M., Roussel, G., Perpète, E. A., Wouters, J., Housen, I., and Michaux, C. (2012) First crystal structure of an endo-inulinase, INU2, from *Aspergillus ficuum*: discovery of an extra-pocket in the catalytic domain responsible for its endo-activity. *Biochimie* **94,** 2423–2430
21. Lammens, W., Le Roy, K., Yuan, S., Vergauwen, R., Rabijns, A., Van Laere, A., Strelkov, S. V., and Van den Ende, W. (2012) Crystal structure of 6-SST/6-SFT from *Pachysandra terminalis*, a plant fructan biosynthesizing enzyme in complex with its acceptor substrate 6-kestose. *Plant J.* **70,** 205–219
22. Alvaro-Benito, M., Polo, A., González, B., Fernández-Lobato, M., and Sanz-Aparicio, J. (2010) Structural and kinetic analysis of *Schwanniomyces occidentalis* invertase reveals a new oligomerization pattern and the role of its supplementary domain in substrate binding. *J. Biol. Chem.* **285,** 13930–13941
23. Lafraya, Á., Sanz-Aparicio, J., Polaina, J., and Marín-Navarro, J. (2011) Fructo-oligosaccharide synthesis by mutant versions of *Saccharomyces cerevisiae* invertase. *Appl. Environ. Microbiol.* **77,** 6148–6157
24. Flint, H. J., Scott, K. P., Louis, P., and Duncan, S. H. (2012) The role of the gut microbiota in nutrition and health. *Nat. Rev. Gastroenterol. Hepatol.* **9,** 577–589
25. Sainz-Polo, M. A., Lafraya, A., Polo, A., Marín-Navarro, J., Polaina, J., and Sanz-Aparicio, J. (2012) Crystallization and preliminary x-ray diffraction analysis of the invertase from *Saccharomyces cerevisiae*. *Acta Crystallogr. F Struct. Biol. Crystal. Commun.* **68,** 1538–1541
26. Battye, T. G. G., Kontogiannis, L., Johnson, O., Powell, H. R., and Leslie, A. G.W. (2011) iMOSFLM: a new graphical interface for diffraction-image processing with MOSFL. *Acta Crystallogr. D* **67,** 271–281
27. Winn, M. D., Ballard, C. C., Cowtan, K. D., Dodson, E. J., Emsley, P., Evans, P. R., Keegan, R. M., Krissinel, E. B., Leslie, A. G. W., McCoy, A., McNicholas, S. J., Murshudov, G. N., Pannu, N. S., Potterton, E. A., Powell, H. R., Read, R. J., Vagin, A., and Wilson, K. S. (2011) Overview of the CCP4 suite and current developments. *Acta Crystallogr. D* **67,** 235–242
28. Stein, N. (2008) CHAINSAW: a program for mutating pdb files used as templates in molecular replacement. *J. Appl. Crystallogr.* **41,** 641–643
29. Murshudov, G. N., Skubák, P., Lebedev, A. A., Pannu, N. S., Steiner, R. A., Nicholls, R. A., Winn, M. D., Long, F., and Vagin, A. A. (2011) REFMAC5 for the refinement of macromolecular crystal structures. *Acta Crystallogr. D* **67,** 355–367
30. Emsley, P., and Cowtan, K. (2004) Coot: model-building tools for molecular graphics. *Acta Crystallogr. D* **60,** 2126–2132
31. Laskowski, R. A., MacArthur, M. W., Moss, D. S., and Thornton, J. M. (1993) PROCHECK: a program to check the stereochemical quality of protein structures. *J. Appl. Crystallogr.* **26,** 283–291
32. Chen, V. B., Arendall, W. B., 3rd, Headd, J. J., Keedy, D. A., Immormino, R. M., Kapral, G. J., Murray, L. W., Richardson, J. S., and Richardson, D. C. (2010) MolProbity: all-atom structure validation for macromolecular crystallography. *Acta Crystallogr. D* **66,** 12–21
33. DeLano, W. L. (2002) *The PyMOL Molecular Graphics System*, DeLano Scientific, San Carlos, CA
34. Krissinel, E., and Henrick, K. (2007) Inference of macromolecular assemblies from crystalline state. *J. Mol. Biol.* **372,** 774–797
35. Williams, R. S., Trumbly, R. J., MacColl, R., Trimble, R. B., and Maley, F. (1985) Comparative properties of amplified external and internal invertase from the yeast *SUC2* gene. *J. Biol. Chem.* **260,** 13334–13341
36. Dou, Y., Baisnée, P. F., Pollastri, G., Pécout, Y., Nowick, J., and Baldi, P. (2004) ICBS: a database of interactions between protein chains mediated by β-sheet formation. *Bioinformatics* **20,** 2767–2777
37. Wasmer, C., Lange, A., Van Melckebeke, H., Siemer, A. B., Riek, R., and Meier, B. H. (2008). Amyloid fibrils of the HET-S(218–289) prion form a β solenoid with a triangular hydrophobic core. *Science* **319,** 1523–1526
38. Guharoy, M., and Chakrabarti, P. (2007) Secondary structure based analysis and classification of biological interfaces: identification of binding motifs in protein-protein interactions. *Bioinformatics* **23,** 1909–1918
39. Álvaro-Benito, M., Sainz-Polo, M. A., González-Pérez, D., González, B., Plou, F. J., Fernández-Lobato, M., and Sanz-Aparicio, J. (2012) Structural and kinetic insights reveal that the amino acid pair Gln-228/Asn-254 modulates the transfructosylating specificity of *Schwanniomyces occidentalis* β-fructofuranosidase, an enzyme that produces prebiotics. *J. Biol. Chem.* **287,** 19674–19686
40. Davies, G. J., Wilson, K. S., and Henrissat, B. (1997) Nomenclature for sugar-binding subsites in glycosyl hydrolases. *Biochem. J.* **321,** 557–559
41. Alvaro-Benito, M., de Abreu, M., Portillo, F., Sanz-Aparicio, J., and Fernández-Lobato, M. (2010) New insights into the fructosyltransferase activity of *Schwanniomyces occidentalis* β-fructofuranosidase, emerging from nonconventional codon usage and directed mutation. *Appl. Environ. Microbiol.* **76,** 7491–7499
42. Conde, R., Cueva, R., Pablo, G., Polaina, J., and Larriba, G. (2004) A search for hyperglycosylation signals in yeast glycoproteins. *J. Biol. Chem.* **279,** 43789–43798
43. Reddy, A. V., MacColl, R., and Maley, F. (1990) Effect of oligosaccharides and chloride on the oligomeric structures of external, internal, and deglycosylated invertase. *Biochemistry* **29,** 2482–2487
44. Gouet, P., Courcelle, E., Stuart, D. I., and Métoz, F. (1999) ESPript: multiple sequence alignments in PostScript. *Bioinformatics* **15,** 305–308

# Three-dimensional Structure of *Saccharomyces* Invertase: ROLE OF A NON-CATALYTIC DOMAIN IN OLIGOMERIZATION AND SUBSTRATE SPECIFICITY

M. Angela Sainz-Polo, Mercedes Ramírez-Escudero, Alvaro Lafraya, Beatriz González, Julia Marín-Navarro, Julio Polaina and Julia Sanz-Aparicio

*J. Biol. Chem. 2013, 288:9755-9766.*
*doi: 10.1074/jbc.M112.446435 originally published online February 21, 2013*